

Cite this: *Nanoscale*, 2014, 6, 2381

Femtosecond laser ablation of highly oriented pyrolytic graphite: a green route for large-scale production of porous graphene and graphene quantum dots†

Paola Russo,^{ab} Anming Hu,^{*ac} Giuseppe Compagnini,^b Walter W. Duley^d and Norman Y. Zhou^a

Porous graphene (PG) and graphene quantum dots (GQDs) are attracting attention due to their potential applications in photovoltaics, catalysis, and bio-related fields. We present a novel way for mass production of these promising materials. The femtosecond laser ablation of highly oriented pyrolytic graphite (HOPG) is employed for their synthesis. Porous graphene (PG) layers were found to float at the water–air interface, while graphene quantum dots (GQDs) were dispersed in the solution. The sheets consist of one to six stacked layers of spongy graphene, which form an irregular 3D porous structure that displays pores with an average size of 15–20 nm. Several characterization techniques have confirmed the porous nature of the collected layers. The analyses of the aqueous solution confirmed the presence of GQDs with dimensions of about 2–5 nm. It is found that the formation of both PG and GQDs depends on the fs-laser ablation energy. At laser fluences less than 12 J cm^{-2} , no evidence of either PG or GQDs is detected. However, polyynes with six and eight carbon atoms per chain are found in the solution. For laser energies in the 20–30 J cm^{-2} range, these polyynes disappeared, while PG and GQDs were found at the water–air interface and in the solution, respectively. The origin of these materials can be explained based on the mechanisms for water breakdown and coal gasification. The absence of PG and GQDs, after the laser ablation of HOPG in liquid nitrogen, confirms the proposed mechanisms.

Received 19th October 2013
Accepted 5th December 2013

DOI: 10.1039/c3nr05572h

www.rsc.org/nanoscale

1. Introduction

Graphene, a two-dimensional (2D) sheet of sp^2 -hybridized carbon atoms, was discovered in 2004.¹ Since then, many studies have been published regarding various methods that have been employed for the synthesis of this promising material for numerous applications.^{1–7} Many advances in this area have involved the growth by chemical vapor deposition (CVD),⁴ liquid phase exfoliation of graphite,⁵ thermal exfoliation⁶ and ultrasonic dispersion⁷ of graphitic oxide. Among these methods, the mechanical exfoliation of highly oriented pyrolytic graphite (HOPG) is considered as one of the most suitable approaches to

obtain high quality graphene sheets. However, due to a low production rate, it is still limited in large-scale applications. Recently, special attention has been paid to graphene-based materials in order to obtain tuneable physical, electronic and mechanical properties. The possibility of using graphene as a membrane for gaseous purification, or for gas storage, has been the focus of the latest energy-related research.^{8–11} In particular, two graphene-based materials appear in the spotlight: porous graphene (PG) and graphene quantum dots (GQDs). PG can be described as a graphene sheet with nanopores originating from the removal of some sp^2 carbon atoms from the plane, leading to applications as a membrane in molecular sieves,¹² as an electrode material for supercapacitors¹³ for energy storage, and as a functional component in nanoelectronics. PG can be obtained by either physical¹⁴ or chemical methods,¹⁵ but techniques that permit bulk scale fabrication are still lacking. GQDs are zero-dimensional materials and have great potential for a variety of uses in photovoltaics,¹⁶ water treatment¹⁷ and other applications.¹⁸ The increasing interest towards these materials is correlated with their unique optical and electronic properties and they differ from graphene due to quantum confinement and edge effects.¹⁹ The GQDs can be regarded as small

^aDepartment of Mechanical and Mechatronics Engineering, University of Waterloo, 200 University Ave., West Waterloo, Ontario N2L 3G1, Canada. E-mail: ahu3@utk.edu

^bDipartimento di Scienze Chimiche, Università degli Studi di Catania, Viale Andrea Doria 6, Catania, 95125, Italy

^cDepartment of Mechanical, Aerospace and Biomedical Engineering, University of Tennessee, Knoxville, TN 37996-2210, USA

^dDepartment of Physics and Astronomy, University of Waterloo, 200 University Ave., West Waterloo, Ontario N2L 3G1, Canada

† Electronic supplementary information (ESI) available. See DOI: 10.1039/c3nr05572h

fragments of graphene sheets with dimensions less than 100 nm. Thus, one of the strategies utilized for their synthesis is to cut graphene sheets into small pieces. The cutting methods employed so far involve the hydrothermal breaking of graphene sheets²⁰ and the photo-Fenton reaction of graphene oxide.²¹ However, these methods for the production of both PG and GQDs are expensive and time consuming since most of them involve many reaction steps.

In this paper, we present a novel, green, scalable and one-pot approach for the synthesis of both porous graphene and graphene quantum dots by the femtosecond laser ablation of HOPG in water. Pulsed laser ablation in liquids is a general approach that facilitates the creation of a large variety of nanomaterials in the colloidal state including metallic particles, metal oxides, semiconductors, and carbon-related materials, depending on the nature of ablated targets.^{22–24} In particular, the laser ablation of carbon in water has been established to be a useful method for the production of solutions of hydrogen-terminated polyynes,^{25–27} *i.e.* linear carbon chains with alternating single and triple bonds. These molecules are usually produced in a vacuum²⁸ as they are unstable and are easily oxidized and/or decomposed in air.^{29–31} On the other hand, linear carbon chains tend to undergo chain-chain cross-linking reactions resulting in sp² graphene structures as a final product.²⁹ However, relatively stable polyynes can be produced by pulse laser ablation of graphite in water and remain well separated in the liquid with lifetimes exceeding 24 hours.³² In addition, the laser heating effect is remarkably localized, which also contributes to the stability of polyyne. Recently, there have been a number of theoretical studies^{33,34} exploring the use of laser pulses for the exfoliation of graphite in order to obtain graphene sheets. In particular, Jeschke *et al.* reported that a femtosecond laser pulse is able to induce strong vibrations of graphite planes that lead to collision of the graphitic planes. Therefore, the planes at the top and the bottom are removed from the surface of the film, causing the exfoliation of graphite.³³ Miyamoto and co-workers demonstrated, *via* TDDFT-MD *ab initio* simulations, that ultrashort laser pulses can be used for the detachment of graphene monolayers from graphite.³⁴ In a previous work, we have reported³⁵ the production of graphene sheets, *via* laser ablation of HOPG in water with nanosecond laser pulses. This approach enabled large-scale production of many graphene sheets that were collected at the water surface. It is long known that femtosecond (fs) and nanosecond (ns) lasers, due to different pulse durations, induce distinct ablation mechanisms.^{36,37} Femtosecond laser pulses transfer energy to electrons of the target material on a time-scale that is much shorter than the electron-phonon thermal process, while nanosecond laser pulses release energy on a time-scale comparable with the thermal relaxation process of the target.²³ Therefore, the induction of thermal effects in ablated materials can be avoided when short-duration pulses³⁸ are used. In addition, the pressure and temperature of the plasma during the fs-ablation in liquids are reported to be as large as 20 000 K and 28 GPa, respectively.³⁹ These values are much higher than those reported for nanosecond laser ablation (4000–5000 K and several GPa, respectively).⁴⁰ Therefore, materials ablated with fs pulses should be dissimilar from those that are produced with longer laser pulses. With this in mind, we have investigated the fs

laser ablation of HOPG in water. We have succeeded in producing porous graphene and GQDs by a green, single step process and an inexpensive way. The main results and the mechanisms proposed to explain the formation of these materials are presented in this paper.

2. Experimental

2.1. Sample preparation

A target of HOPG (ZYH from Momentive Performance) was placed at the bottom of a quartz cell filled with water (Millipore grade water, 18 MΩ m) and a femtosecond laser (1 kHz, 800 nm, Coherent Inc.) with a pulse duration of 35 fs was used for ablation of the target. The laser beam was deflected by 90° by means of mirrors in order to perform the ablation of the target from the top of the water layer. HOPG was continuously ablated for 20 minutes at a constant fluence. Within the range of 20–30 J cm⁻², slight black films were formed and covered the whole water surface and at the same time, the solution changed into a grey color. The floating film was collected onto silicon wafers with a certain thickness of silicon dioxide (285 nm in thickness from Graphene Laboratories Inc.) for optical imaging analysis. The solution was dripped onto Si wafer and subsequently dried for microstructure characterization.

2.2. Instrumentation

Ultraviolet-visible (UV-VIS) analysis of solutions, obtained after laser processing, was carried out with a Shimadzu UV-2100 PC spectrophotometer over a spectral range of 190–500 nm. The optical imaging analysis of the floating layers was performed by means of an optical microscope (Nikon BX) with 10×, 20×, and 50× objectives. The layers were analyzed using a Renishaw In Via micro-Raman spectrometer, employing an excitation laser with a wavelength of 633 nm, and the spectra were acquired with a 50× objective at a laser power of 0.1 mW. A field emission scanning electron microscope (FE-SEM, Magellan 400) was used to analyze the structure of the layers recovered at the water–air interface. The layer morphology was investigated with an atomic force microscope (Parks system NSOM model). In order to study the layer chemistry, X-ray photoelectron spectroscopy (XPS) analysis was carried out using a multi-technique ultra-high vacuum imaging XPS microprobe spectrometer (Thermo VG Scientific ESCALab 250) with a monochromatic Al-Kα 1486.6 eV X-ray source. The spectrometer was calibrated by Au 4f7/2 (binding energy of 84.0 eV) with respect to the Fermi level. The chamber vacuum level was maintained below 2 × 10⁻¹⁰ Torr.

3. Results and discussion

3.1. Formation of porous graphene (PG)

Solutions obtained after the laser ablation experiments, performed at 25 J cm⁻², showed the presence of a large amount of material in the form of layers floating at the water–air interface. These layers, recovered onto suitable substrates, were first characterized by optical microscopy, which permits the distinction of a single layer graphene sheet (SLG) from bi- or

multi-layers of graphene as a result of different contrasts. The single layer usually appears as a light blue sheet, and the color becomes darker as the number of layers increases.⁴¹ In the present work, the layers have been collected onto a silicon substrate with a 285 nm silicon dioxide layer as reported in the sample preparation section. The optical images of the sheets, shown in Fig. 1a and b, clearly demonstrate that the fs laser ablation of HOPG, compared to the case of the nanosecond laser,³⁵ induced the exfoliation of graphite and yielded large graphene sheets located at the water–air interface. The average dimensions of the floating layers were found to be in the range of ~ 100 – 200 μm , and once they have been collected onto the substrate, they appeared as a uniform veil. However, a small amount of multi-layers and some pieces of graphite were also produced, as indicated by a contrast difference in Fig. 1a. Layers detached by the laser process displayed a corrugated surface and some folds were also visible, as shown in Fig. 1b. The presence of these bends is likely to be related to the deposition procedure of these ultrathin layers onto the silicon substrate since these layers floating at the water–air interface were picked up using the silicon substrate at the end of the laser process. This rough collection method is expected to lead to the corrugation of the surface of the resulting layers. Moreover, the layers also exhibited a discontinuous surface where some holes were detected as clearly seen in the higher magnification inset of Fig. 1b. The atomic force microscopy (AFM) analysis was carried out in order to determine the morphology and the number of these layers. In Fig. S1 (see ESI[†]), a topographic image of a layer and its relative height profile are displayed. We can define the edges of the analyzed layer from AFM images, proving that the collected materials consisted of layers with well-defined borders and that they were not agglomerated nanoparticles.

This point is further supported by a post-treatment with ultra-sonication, which did not break these sheets into individual particles. However, AFM data confirm the irregular

nature of the sheet, even though it is not able to give the exact number of layers involved, because of the significant roughness and a limited lateral resolution. From the height profile (on the right of Fig. S1[†]), the step between the substrate and the layer is ~ 10 nm corresponding to ~ 30 layers, as the interlayer distance in graphite is 0.34 nm. It is clear that this number of layers is over estimated from the sheet roughness.

To further elucidate the layer structure, field emission scanning electron microscopy imaging analysis was performed on the samples as shown in Fig. 1c and d. Fig. 1c shows an overview of the suspended layers collected on the silicon substrate. It is easy to identify either layers with dimensions of ~ 100 μm covering a large area of substrate or smaller pieces about 10–20 μm in size that appear very close together so that they almost form a continuous layer. The bigger sheets exhibited many ripples on the surface, while the smaller ones appear almost flat at the same magnification. The area inside the yellow circle was then examined at increased magnification, as shown in Fig. 1d. The irregular composition of these layers indicates that they have a three-dimensional (3D) porous structure. The pores are ~ 10 – 20 nm in size as shown in the inset. This porosity may be the cause of the overestimation of the height of these layers as determined from AFM analysis. All the layers collected exhibited this spongy structure independent of the size or thickness of the layer. Fig. S2[†] shows an FE-SEM image of a single layer of graphene, where many ~ 20 nm holes are visible. Thus, porous graphene can be described as a graphene sheet with nanopores created by the removal of carbon atoms from the plane. From SEM analysis, it is evident that all sheets detached by the laser ablation process exhibit a homogeneously porous structure. Transmission electron microscopy (TEM) images of these layers are shown in Fig. 2. TEM samples were collected by a lacey carbon coated copper grid, and subsequently dried naturally. Fig. 2a indicates the presence of structures with varying number of folded layers (between one and five) and the presence of ripples, as seen by FE-SEM and optical microscopy.

The interlayer d -spacing of 0.34 nm was found to be the same as reported for graphite.⁴² Fig. 2b shows a TEM image of a single layer of porous graphene, where the d -spacing was calculated to be 0.21 nm, corresponding to the distance of the zigzag (C–C–C)

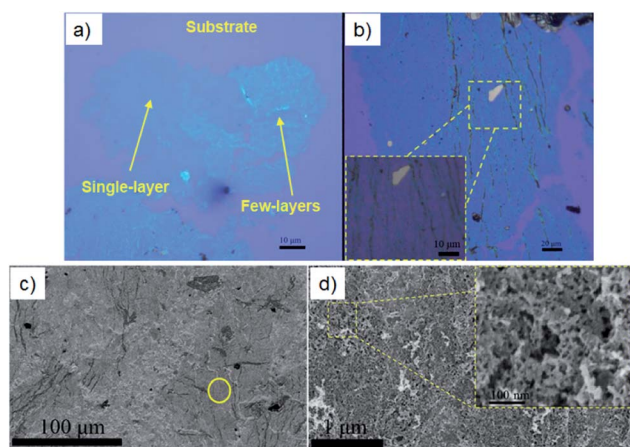


Fig. 1 (a) and (b) Optical images of graphene layers. (a) Single and a few-layers are indicated with yellow arrows. (b) A layer displaying ripples is shown. (c) and (d) Field emission SEM images (FE-SEM): (c) overview of layers deposited onto the substrate. (d) High magnification of the area marked with a circle in (c), showing the porous structure of the layers.

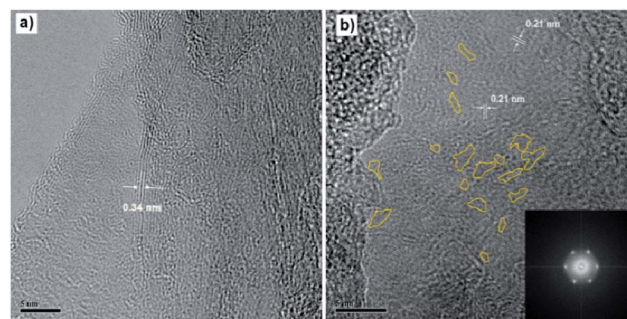


Fig. 2 TEM images of the folded graphene layers (a) floating at the water–air interface. (b) TEM image of a single layer of porous graphene. A 2D FFT of this image is reported in the inset, and the pores on the graphene sheet are highlighted by yellow loops.

chains in graphite.⁴² A 2D fast Fourier transform (FFT) was performed on this image and the results are shown in the inset of Fig. 2b. The FFT showed only six spots in a hexagonal pattern with 0.21 nm spacing, confirming the monolayer structure of graphene, consistent with prior reports.^{43,44} Previous TEM studies have demonstrated the possibility of identifying the presence of defects in terms of mono- or multi-vacancies on the graphene plane.^{43,45–47} Fig. 2b highlights some areas where missing rows of carbon atoms can be observed. This confirms the presence of nanoholes or nanopores within the graphene network, and provides supporting evidence for the formation of porous graphene by fs ablation. Fig. S3† shows the highlighted area in Fig. 2b where the missing rows can be easily distinguished. It is significant that all the layers recovered from solution have this porous structure, thus confirming the fact that the present technique is a simple, green, and scalable method for the exfoliation of graphite and the production of porous graphene.

3.2. Formation of graphene quantum dots

Following the fs ablation and after the removal of the floating sheets, the solutions were analyzed by means of absorption spectroscopy. The main results are shown in Fig. 3. The absorption spectrum of the obtained solution after laser ablation at 25 J cm^{-2} revealed the presence of an absorption peak centered at 270 nm. This peak was also detected in solutions prepared with nanosecond laser pulses,³⁵ and can be attributed to the presence of GQDs⁴⁸ or graphene nanosheets⁴⁹ as it arises from the excitation of a π -plasmon resonance in the graphitic structure.⁵⁰ It is significant that only the signal at 270 nm was detected, while with longer pulses, the spectra also showed absorption bands at 225 nm and 215 nm arising from polyynes.³⁵ Recently, several groups reported that GQDs produced with different methods display photoluminescence properties.⁵¹ The luminescence mechanism of GQDs is not fully understood and it may derive from intrinsic state emission and defect state emission. In order to investigate the photoluminescence properties of our GQDs, we performed the PL analysis of the solution

and the obtained spectrum is reported in Fig. 3 (blue line). Excitation has been performed at 270 nm (absorption maximum) and PL show a single signal at 297 nm which is blue shifted with respect to the emission of the GQDs produced with other methods. In general, depending on the synthetic path, GQDs can show blue, green, yellow and red luminescence, and it was reported that the PL emission in GQDs could be size-, excitation-, solvent-dependent. In particular, a decrease of the GQD size leads to a blue shift of the luminescence emission. In our case, it seems that we were able to produce smaller GQDs. For TEM characterization, some drops of the solution were deposited onto a copper grid.

The results are shown on the right side of Fig. 3. The presence of graphene quantum dots with dimensions in the order of 2–5 nm is clearly seen in this image (see the inset), in accordance with the PL results. The measured d -spacing was 0.23 nm, which agrees well with that reported in the literature for graphene.^{43,44,52} The GQDs are embedded within an amorphous matrix, and some wrapped graphene sheets were also detected, suggesting that some graphene sheets remain dispersed in the liquid. Based on these results, we conclude that the GQDs dispersed in water gave rise to the absorption band at 270 nm. A similar conclusion was reported by Zhou *et al.*⁴⁸ The fs laser ablation experiments were also performed using lower fluence. In particular, the HOPG target was ablated with a fluence of $\sim 10 \text{ J cm}^{-2}$, and neither the PG layers nor the GQDs were subsequently detected in the aqueous solution. Under these conditions, the absorption spectrum of the solution showed the presence of hydrogen-terminated polyynes containing six and eight carbon atoms per chain. This suggests that the formation of both PG and GQDs depends on the laser energy during the ablation experiments. In particular, we found that, in the range of $5\text{--}12 \text{ J cm}^{-2}$, polyynes (C_6 and C_8) are produced, while for fluences $>20 \text{ J cm}^{-2}$, porous graphene and GQDs are obtained, without detectable quantities of polyynes. The yield of GQDs is estimated to reach 16 mg L^{-1} after 20 minutes of irradiation at 20 J cm^{-2} . The effect of the ablation duration on the optimized yields of PG and GQDs will be elucidated below, together with the AFM analysis of GQDs in order to determine the heights of these systems.^{53,54}

The solution of GQDs was then analyzed by IR spectroscopy and the results are displayed in Fig. 4. In particular, for comparison, it has been reported the IR spectrum of the solution containing the GQDs (c), the IR spectrum of GO produced by the Hummers method (a) and the IR spectrum of reduced GO (b). It is easy to see that the GQDs obtained after the PLA in water show the presence of two peaks representing the asymmetric and symmetric CH_2 stretching vibrations at 2923 cm^{-1} and 2850 cm^{-1} , respectively. These peaks are absent in the spectrum of GO and they are slightly evident in the reduced GO. If we look at the spectra of GO and rGO, the presence of the following features is notable: a peak representing the stretching of carbonyl groups ($\text{C}=\text{O}$) at 1739 cm^{-1} , a peak representing the stretching of aromatic ethers (aryl-o) observed at 1310 cm^{-1} to 1210 cm^{-1} and the peak of the O–H stretching in aromatic rings in the $1260\text{--}1000 \text{ cm}^{-1}$ region. These peaks are absent in the spectrum of GQDs, confirming that the GQDs produced by PLA

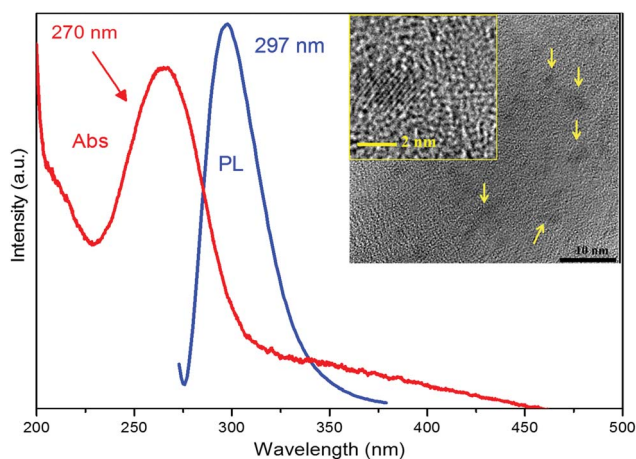


Fig. 3 Absorption spectrum (red), PL spectrum (blue) and TEM images of the solid component in the solution after fs ablation at 25 J cm^{-2} .

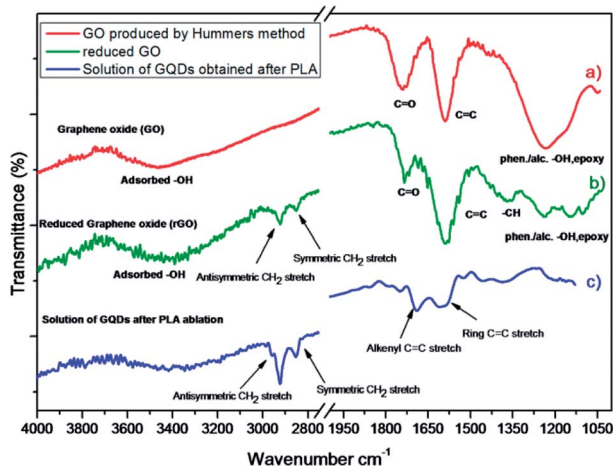
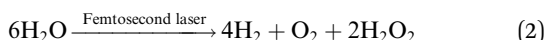
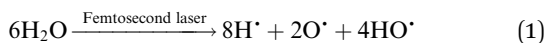


Fig. 4 IR spectra of GO (a), reduced GO (b) and the solution of GQDs (c) obtained after fs ablation at 25 J cm^{-2} .

in water do not show the presence of oxygen groups bonded to the carbon atoms. In the spectrum of GQDs two peaks are detected at 1685 cm^{-1} and 1597 cm^{-1} representing the alkenyl C=C stretching and the ring stretching in benzene derivatives, respectively.

3.3. Mechanisms for the production of PG and GQDs

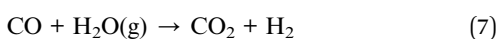
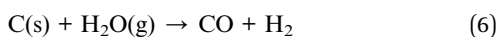
In order to explain the formation of either PG or GQDs, two primary related mechanisms should be considered. These involve laser-induced water breakdown and a laser-induced mechanism similar to that occurring in the coal gasification process. When a fs-laser is focused onto water, laser ionization and photo-dissociation of water molecules leads to the formation of H, O and OH radicals as indicated in reaction (1).⁵⁵ Subsequent reactions result in the formation and evolution of H_2 and O_2 as well as H_2O_2 which acts as a strong oxidizer.



The second mechanism, related to the decomposition of water, is called the coal gasification. This process occurs when solid carbon-based materials (C(s)) react with oxygen, steam, carbon dioxide, and hydrogen to produce fuel-rich products.⁵⁶ The reaction can be expressed as:



Any free oxygen rapidly reacts with CO in the gas phase to produce CO_2 , according to reaction (4):



These reactions, acting collectively, are suggested as the mechanism leading to the formation of porous graphene in the present experiments and are initiated by the decomposition of water associated with the femtosecond laser ablation. The water breakdown is the first crucial step, producing the reactive species O_2 , H_2 , and H_2O_2 . Simultaneously, the laser pulses exfoliate the graphite, causing the detachment of graphene sheets. Subsequently, O_2 and the H_2O_2 molecules oxidize the graphene sheets, forming several layers of graphene oxide (GO), in which carbon atoms possess sp^3 hybridization due to their bonds with oxygen atoms. In the second important step, the sp^3 carbon atoms of the GO sheet react with oxidized species, in a way similar to the coal gasification mechanism of solid carbon. This reaction leads to the formation of CO and CO_2 molecules, which leave behind a distribution of carbon vacancies and creating nanopores. As a result, porous graphene is produced and it floats toward the water-air interface where it can be easily collected and characterized. Recently, Koinuma and coworkers have reported⁵⁷ the production of nanopores in GO sheets, *via* photoreaction in O_2 under UV irradiation. In their work, they demonstrated that, for the formation of pores, carbon atoms with sp^3 hybridization must be present, as no pores were produced when sp^2 hybridized graphene sheets were subjected to the same photoreaction in O_2 . The mechanisms proposed here show that the first crucial step for the synthesis of porous graphene is the breakdown of water, since it produces O_2 and H_2O_2 that leads to the formation of GO, without which porous graphene cannot be formed. This step is confirmed by the observation of laser filamentation formation in water during fs laser exfoliation. The second important step is the reaction between sp^3 carbon atoms in the GO sheets with O_2 , which leads to the formation of the pores. X-ray photoelectron spectroscopy (XPS) analysis of the recovered layers is shown in Fig. S4.† The spectrum is similar to that reported for graphene sheets having a very low content of oxygen.³⁵ This indicates that GO sheets formed during the experiments are completely converted into PG as an intermediate step by the coal gasification mechanism.

Noteworthy, in the experiments with a ns laser, the sheets appeared to be almost flat without any evidence of pores.³⁵ These different results can be attributed to the absence of the hydrogen peroxide in the water solution and a relatively low lattice temperature during the nanosecond laser ablation. Chin S. L. reported that when a nanosecond laser is focused into water producing breakdown, only O_2 and H_2 are detected, since H_2O_2 molecules are dissociated by the shock waves of the plasma.⁵⁵ Therefore, in the absence of hydrogen peroxide, graphene sheets exfoliated by ns laser pulses are subject to a lower oxidation rate than is the case with fs laser irradiation. Indeed, in our previous work,³⁵ we demonstrated that the sheets obtained were reduced GO sheets and that sp^2 domains were still detectable. This suggests that the concentration of sp^3 carbon atoms was small so that the coal gasification process was inhibited. With a focused fs beam, the intensity is $\sim 10^{14} \text{ W cm}^{-2}$ so that liquid molecules are readily ionized.²⁷ For the coal gasification, operating temperature, operating pressure, coal particle size, and O_2/coal ratio are key process variables. In

particular, a decrease in the coal size requires a higher O_2 /coal ratio and very high operating temperatures⁵⁶ (up to 2200 K in oxygen-blown gasifiers). Considering these factors, *e.g.* the liquid environment, the small quantity of material produced, and the presence of $\sim 3 \times 10^{-7}$ mol⁵⁵ of O_2 , it seems that the temperature reached during the ns laser ablation experiments (~ 4000 – 5000 K) is not high enough to obtain the gasification reaction of the sp^3 carbon atoms in the graphene layers. Instead, when ultrashort pulses are used, not only hydrogen peroxide is produced, which leads to stronger oxidation of the layers, but the possibility of reaching $\sim 20\,000$ K permits the coal gasification reaction of the graphene oxide sheets and the formation of PG. The formation of GQDs is then a natural consequence of the continuing gasification of PG. During fs ablation, many layers are detached from the HOPG target. These sheets are more easily oxidized *via* the reactions described above. As a result of the coal gasification process, many holes are formed. The continuing destruction of porous graphene results in very small GQD fragments dispersed in water. This is consistent with the reported approaches for the synthesis of GQDs by cutting GO layers with suitable reactants.^{20,21}

3.4. Experiments in liquid nitrogen (N_2)

In order to prove the validity of these mechanisms, femtosecond laser ablation of HOPG was carried out in liquid nitrogen (N_2). The experiments were set at the same fluence (25 J cm^{-2}) and time (20 minutes) employed for the experiments in water. The products of the ablation were collected at the end of the laser ablation by submerging a substrate of Si/SiO₂ in the remaining liquid nitrogen and waiting for its evaporation. In this way, the materials produced were allowed to deposit on the top of the substrate and then characterized by means of optical microscopy, FE-SEM, and Raman spectroscopy. Fig. 5 shows the results of FE-SEM analysis. The analysis of the samples using the optical microscope (Fig. S5†) showed that the exfoliation of HOPG is possible in liquid N_2 . Most of the detached layers were thicker than the ones obtained in water and a large quantity of graphitic materials covered the layers.

However, the dimensions of the detached layers ($\sim 100\ \mu\text{m}$) were found to be comparable to those obtained after fs ablation in water (see Fig. S5†). The fs ablation of HOPG in liquid N_2 seems to have a higher ablation rate together with less efficient exfoliation. Fig. 5 shows the FE-SEM image of a thin sheet, where the edges are clearly visible together with superimposed graphitic materials. The absence of ripples suggests that the improved way to deposit the layers is by placing the substrate at the bottom of the quartz cell and allowing the evaporation of the solvent. The inset of Fig. 5 shows a high magnification SEM image of the area indicated with a dashed yellow box. It is obvious that the layer did not show the presence of pores, proving the validity of the mechanisms proposed above. Hence, for the synthesis of porous graphene, both O_2 and H_2O_2 are necessary. After the evaporation of the liquid nitrogen, we also observed some materials attached to the walls of the beaker. These materials were recovered with water and analyzed by means of absorption spectroscopy. The results are shown in

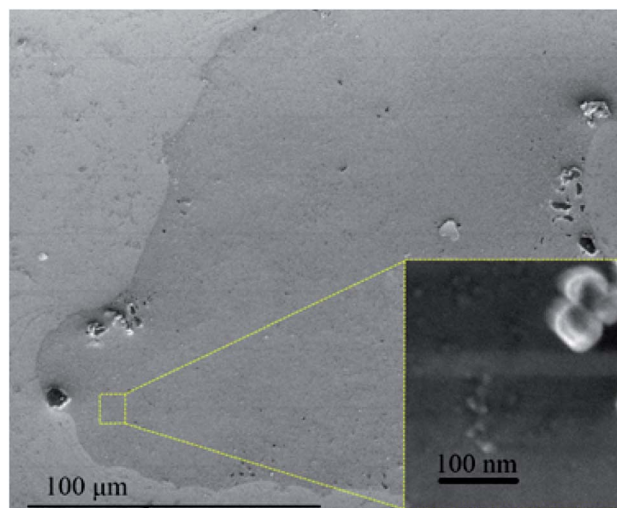


Fig. 5 SEM image of a layer obtained after fs laser ablation of HOPG in liquid N_2 . The inset shows a magnification of the area inside the yellow dashed box.

Fig. 6a. The absorption spectrum shows the presence of four absorption bands at 223, 235, 247, and 260 nm respectively, which can be attributed to cyanopolynes.^{58–60} These systems are polyne chains ending with a cyanide functional group, and generally, they are produced by arc discharge in liquid nitrogen,⁵⁸ or found in the interstellar medium.^{59,61} Comparing the absorption bands reported in the literature⁵⁸ with those for our solutions, it is apparent that the fs-ablation of HOPG in liquid N_2 results in the synthesis of cyanopolynes containing eight carbon atoms per chain (C_8N_2). It was also found that the synthesis of cyanopolynes was dependent on fluence. In particular, large quantities of these molecules can be produced with fluences in the range between 20 and 30 J cm^{-2} , while for lower values (10 – 15 J cm^{-2}), no cyanopolynes were detected. These results can be attributed to the strong femtosecond laser pulse being able to directly ionize N_2 molecules. The nitrogen ion can attach to polyynes and can form the stable cyanopolynes. To our knowledge, the fs laser ablation in liquid nitrogen has not yet been reported as a technique for the

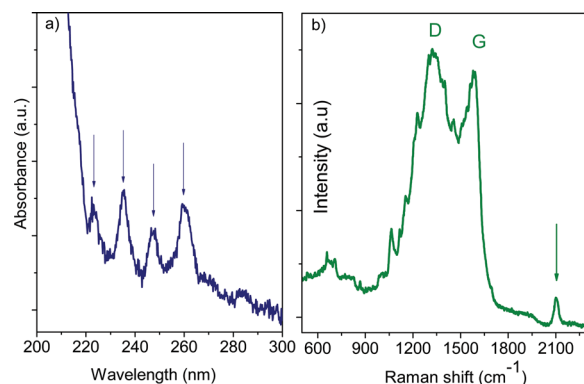


Fig. 6 (a) Absorption spectrum of the solution obtained after fs-ablation of HOPG in N_2 ; and (b) SERS of the solution.

synthesis of cyanopolynes, suggesting that this is a novel and facile route for their production.

The samples were then characterized by Raman spectroscopy. Generally, the Raman signals of polyynes are very weak, therefore, we employed the surface enhanced Raman spectroscopy (SERS) technique.^{62,63} This is known to increase the Raman signals from molecules that are attached to metallic nanostructures. In the present work, for the SERS characterization, some drops of silver nanoparticle solution were first deposited onto a glass substrate.

The Raman spectrum shown in Fig. 6b was then collected after dripping a drop of solution onto silver colloid film. The spectrum displayed in Fig. 6b shows the presence of a band at 2100 cm⁻¹, which can be attributed to the presence of polyynes. Indeed, Raman bands located around 1800–2100 cm⁻¹ are related to sp-hybridized linear carbon chains of different lengths.^{64,65} The band found at 2100 cm⁻¹ suggests the presence of polyynes with eight carbon atoms per chain,⁶⁴ in accordance with the UV-VIS results. Between 1200 and 1600 cm⁻¹, the D and G peaks, rising from the vibrations of sp² carbon atoms, are visible. The shape of these peaks suggests that the material analyzed consisted of disordered graphite and other carbon nanostructures.^{66,67} It should be noted that, even if the fs-laser ablation is performed in N₂, some water molecules can still be present due to the adsorbed water. However, the amount of water is pretty low, and the concentration of the reactive species formed during water breakdown is not high enough to initiate the reaction for the formation of PGs. Nevertheless, some trace hydrogen is present and the spectral peaks at frequencies of ~657, 707, and 866 cm⁻¹ can be attributed to the out-of-plane (oop) bending modes of CH groups in polycyclic aromatic hydrocarbon (PAH) molecules.^{68–70} It has been reported that the energies of these oop vibrations depend on the number of adjacent CH groups.⁶⁸ In particular, the observed signals at 707 and 866 cm⁻¹ can be attributed to quintet and duo groups^{71,72} respectively, while the peak at ~650 cm⁻¹ can be assigned to the oop vibrations of benzene.⁷¹ The presence of these molecules can be attributed to the crosslinking of polyynes into PAHs,⁵⁹ as it is known and accepted that polyynes can be used as precursors for PAH formation.⁷³

4. Conclusions

In summary, we have developed a novel, scalable and green method for the synthesis of either PG or GQDs by femtosecond laser ablation of HOPG in water. PG was found to float at the water–air interface, while GQDs were dispersed in the solution. The suspended layers showed a pore dimension of ~20 nm, while GQDs displayed dimensions of about 2–5 nm. The fs ablation of HOPG led to the exfoliation of graphene layers, which are then oxidized to GO layers by O₂ and H₂O₂ produced by the femtosecond laser-induced breakdown of water. The sp³ carbon atoms of the GO layers reacted simultaneously with O₂ in a way similar to that occurring in the coal gasification process. Consequently, CO and CO₂ molecules are formed leaving carbon vacancies and creating nanopores and PG. Experiments performed in liquid nitrogen have confirmed these

proposed mechanisms as PG and GQDs are not formed in the absence of O₂ and H₂O₂, the key reagents for the formation of both materials. Moreover, cyanopolynes were formed during the fs ablation of HOPG in liquid nitrogen. To our knowledge, this is the first use of fs ablation for the production of porous graphene, performed in water, and for the production of cyanopolynes with ablation achieved in liquid N₂. During the paper layout, we found that Habiba⁷⁴ and coworkers reported the synthesis of luminescent GQDs by pulsed laser ablation. The authors employed a nanosecond laser and synthesized the GQDs irradiating a suspension of nickel oxide in benzene. In this respect, our method seems to be simpler and greener compared to Habiba's one, since we are able to obtain GQDs directly in water avoiding the use of a catalyst and benzene.

Acknowledgements

The work is supported by the Natural Science and Engineering Council of Canada (NSERC, Canada).

Notes and references

- 1 K. S. Novoselov, A. K. Geim, S. V. Morozov, D. Jiang, Y. Zhang, S. V. Dubonos, I. V. Grigorieva and A. A. Firsov, *Science*, 2004, **306**, 666–669.
- 2 A. K. Geim and K. S. Novoselov, *Nat. Mater.*, 2007, **6**, 183–191.
- 3 M. Zhou, Y. M. Zhai and S. J. Dong, *Anal. Chem.*, 2009, **81**, 5603–5613.
- 4 A. Reina, A. Jia, X. Ho, J. Nezich, D. Son, H. Bulovic, V. Dresselhaus, M. S. Kong and J. Large Area, Few-Layer Graphene Films on Arbitrary Substrates by Chemical Vapor Deposition, *Nano Lett.*, 2009, **9**, 30–35.
- 5 Y. Hernandez, V. Nicolosi, M. Lotya, F. M. Blighe, Z. Sun, S. De, I. T. McGovern, B. Holland, M. Byrne and Y. K. Gun'Ko, *Nanotechnology*, 2008, **3**, 563–568.
- 6 H. C. Schniepp, J. L. Li, M. J. McAllister, H. Sai, M. Herrera-Alonso, D. H. Adamson, R. K. Prud'homme, R. Car, D. A. Saville and I. A. Aksay, *J. Phys. Chem. B*, 2006, **110**, 8535–8539.
- 7 S. Niyogi, E. Bekyarova, M. E. Itikis, J. L. McWilliams, M. A. Hammon and R. C. Haddon, *J. Am. Chem. Soc.*, 2006, **128**, 7720–7721.
- 8 J. S. Bunch, S. S. Verbridge, J. S. Alden, A. M. van der Zande, J. M. Parpia, H. G. Craighead and P. L. McEuen, *Nano Lett.*, 2008, **8**, 2458–2462.
- 9 S. Patchkovskii, J. S. Tse, S. N. Yurchenko, L. Zhechkov, T. Heine and G. Seifert, *Proc. Natl. Acad. Sci. U. S. A.*, 2005, **102**, 10439–10444.
- 10 K. S. Novoselov, A. K. Geim, S. V. Morozov, D. Jiang, M. I. Katsnelson, I. V. Grigorieva, S. V. Dubonos and A. A. Firsov, *Nature*, 2005, **438**, 197–200.
- 11 Z. Yang, R. G. Gao, N. T. Hu, J. Chai, Y. W. Cheng, L. Y. Zhang, H. Wei, E. S.-W. Kong and Y. F. Zhang, *Nano-Micro Lett.*, 2012, **4**, 1–9.
- 12 S. P. Koenig, L. Wang, J. Pellegrino and J. S. Bunch, *Nat. Nanotechnol.*, 2012, **7**, 728–732.

- 13 L. L. Zhang, X. Zhao, M. D. Stoller, Y. Zhu, H. Ji, S. Murali, Y. Wu, S. Perales, B. Clevenger and R. S. Ruoff, *Nano Lett.*, 2012, **12**, 1806–1812.
- 14 D. C. Bell, M. C. Lemme, L. A. Stern, J. R. Williams and C. M. Marcus, *Nanotech.*, 2009, **20**, 455301–455306.
- 15 F. Zhuangjun, Z. Qiankun, L. Tianyou, Y. Jun, R. Yueming, F. Jing and W. Tong, *Carbon*, 2012, **50**, 1699–1712.
- 16 V. Gupta, N. Chaudhary, R. Srivastava, G. D. Sharma, R. Bhardwaj and S. Chand, *J. Am. Chem. Soc.*, 2011, **133**, 9960–9963.
- 17 S. Zhuo, M. Shao and S. T. Lee, *ACS Nano*, 2012, **6**, 1059–1064.
- 18 L. Li, G. Wu, G. Yang, J. Peng, J. Zhao and J.-J. Zhu, *Nanoscale*, 2013, **5**, 4015–4039.
- 19 L. A. Ponomarenko, F. Schedin, M. I. Katsnelson, R. Yang, E. W. Hill, K. S. Novoselov and A. K. Geim, *Science*, 2008, **320**, 356–358.
- 20 D. Pan, J. Zhang, Z. Li and M. Wu, *Adv. Mater.*, 2010, **22**, 734–738.
- 21 X. Zhou, Y. Zhang, C. Wang, X. Wu, Y. Yang, B. Zheng, H. Wu, S. Guo and J. Zhang, *ACS Nano*, 2012, **6**, 6592–6599.
- 22 F. Mafune, J. Y. Kohno, Y. Takeda and T. Kondow, *J. Phys. Chem. B*, 2003, **107**, 4218–4223.
- 23 V. Amendola and M. Meneghetti, *Phys. Chem. Chem. Phys.*, 2009, **11**, 3805–3821.
- 24 G. W. Yang, J. B. Wang and Q. X. Liu, *J. Phys.*, 1998, **10**, 7923–7927.
- 25 G. Compagnini, V. Mita, L. D'Urso, R. S. Cataliotti and O. Puglisi, *J. Raman Spectrosc.*, 2008, **39**, 177–181.
- 26 S. K. Shin, J. K. Song and S. M. Park, *Appl. Surf. Sci.*, 2011, **257**, 5156–5158.
- 27 A. Hu, J. Sanderson, A. A. Zaidi, C. Wang, T. Zhang, Y. Zhou and W. W. Duley, *Carbon*, 2008, **46**, 1823–1825.
- 28 A. Hu, M. Rybachuk, Q.-B. Lu and W. W. Duley, *Appl. Phys. Lett.*, 2007, **91**, 131906–131913.
- 29 L. Kavan, *Carbyne and Cabynoid Structures*, ed. R. B. Heimann, S. E. Evsyukov and L. Kavan, Kluwer Academic Publishers, 1999, p. 444.
- 30 L. Kavan, *Chem. Rev.*, 1997, **97**, 3061–3082.
- 31 T. Henning and F. Salama, *Science*, 1998, **282**, 2204–2210.
- 32 S. K. Shin and S. M. Park, *Bull. Korean Chem. Soc.*, 2012, **33**, 597–600.
- 33 H. O. Jeschke, M. E. Garcia and K. H. Bennemann, *Phys. Rev. Lett.*, 2001, **87**, 015003–015004.
- 34 Y. Miyamoto, H. Zhang and D. Tománek, *Phys. Rev. Lett.*, 2010, **104**, 208302.
- 35 G. Compagnini, P. Russo, F. Tomarchio, O. Puglisi, L. D'Urso and S. Scalese, *Nanotechnology*, 2012, **23**, 505601.
- 36 B. N. Chichkov, C. Momma, S. Nolte, F. von Alvensleben and A. Tiinnermann, *Appl. Phys. A*, 1996, **63**, 109–115.
- 37 L. Jiang and H. L. Tsai, *Proceeding of NSF Workshop on Research Needs in Thermal Aspects of Material Removal*, Stillwater, 2003, pp. 163–177.
- 38 A. Santagata, A. De Bonis, A. De Giacomo, M. Dell'Aglio, A. Laurita, G. S. Senesi, R. Gaudiuso, S. Orlando, R. Teghil and G. P. Parisi, *J. Phys. Chem. C*, 2011, **115**, 5160–5164.
- 39 D. Perez, L. K. Beland, D. Deryng, L. J. Lewis and M. Meunier, *Phys. Rev. B: Condens. Matter Mater. Phys.*, 2008, **77**, 014108.
- 40 G. W. Yang, *Prog. Mater. Sci.*, 2007, **52**, 648–698.
- 41 Z. H. Ni, H. M. Wang, J. Kasim, H. M. Fan, T. Yu, Y. H. Wu, Y. P. Feng and Z. X. Shen, *Nano Lett.*, 2007, **7**, 2758–2763.
- 42 J. H. Knox, K. Bulvinder and G. R. Millward, *J. Chromatogr.*, 1986, **352**, 3–25.
- 43 J. H. Warner, M. H. Rummeli, A. Bachmatiuk and B. Buchner, *Nanotechnology*, 2010, **21**, 325702.
- 44 J. H. Warner, F. Schaffel, M. H. Rummeli and B. Buchner, *Chem. Mater.*, 2009, **21**, 2418–2421.
- 45 T. Takamura, K. Endo, L. Fu, Y. Wu, K. J. Lee and T. Matsumoto, *Electrochem. Acta*, 2007, **53**, 1055–1061.
- 46 A. Hashimoto, K. Kazusuenaga, A. Gloter, K. Urita and S. Iijima, *Nature*, 2004, **430**, 870–873.
- 47 J. C. Meyer, C. Kisielowski, R. Erni, M. D. Rossell, M. F. Crommie and A. Zettl, *Nano Lett.*, 2008, **8**, 3582–3586.
- 48 J. Zhou, C. Booker, R. Li, X. Zhou, T.-K. Sham, X. Sun and Z. Ding, *J. Am. Chem. Soc.*, 2007, **129**, 744–745.
- 49 M. Feng, R. Sun, H. Zhan and Y. Chen, *Nanotechnology*, 2010, **21**, 075601.
- 50 G. Wang, X. Shen, J. Yao and J. Park, *Carbon*, 2009, **47**, 2049–2053.
- 51 L. Li, G. i. Wu, G. Yang, J. Peng, J. Zhao and J.-J. Zhu, *Nanoscale*, 2013, **5**, 4015–4039.
- 52 L. Lin and S. Zhang, *Chem. Commun.*, 2012, **48**, 10177–10179.
- 53 S. Zhu, J. Zhang, X. Liu, B. Li, X. Wang, S. Tang, Q. Meng, Y. Li, C. Shi, R. Hu and B. Yang, *RSC Adv.*, 2012, **2**, 2717–2720.
- 54 S. Zhu, S. Tang, J. Zhang and B. Yang, *Chem. Commun.*, 2012, **48**, 4527–4539.
- 55 S. L. Chin and S. Lagace, *Appl. Opt.*, 1996, **35**, 907–911.
- 56 L. D. Smoot and P. J. Smith, *Gasification of Coal in Practical Flames*, in *Coal Combustion and Gasification*, ed. D. Luss, Plenum Press, New York, 1985, pp. 151–162.
- 57 M. Koinuma, C. Ogata, Y. Kamei, K. Hatakeyama, H. Tateishi, Y. Watanabe, T. Taniguchi, K. Gezuhara, S. Hayami, A. Funatsu, M. Sakata, Y. Kuwahara, S. Kurihara and Y. Matsumoto, *J. Phys. Chem. C*, 2012, **116**, 19822–19827.
- 58 F. Cataldo, *Polyhedron*, 2004, **23**, 1889–1896.
- 59 F. Cataldo, *Int. J. Astrobiol.*, 2004, **3**, 237–246.
- 60 F. Cataldo, *Tetrahedron*, 2004, **60**, 4265–4274.
- 61 P. Ehrenfreund and S. B. Charnley, *Annu. Rev. Astron. Astrophys.*, 2000, **38**, 427–483.
- 62 D. Nishide, T. Wakabayashi, T. Sugai, R. Kitaura, H. Kataura, Y. Achiba and H. Shinohara, *J. Phys. Chem. C*, 2007, **111**, 5178–5183.
- 63 H. Tabata, M. Fujii and S. Hayashi, *Chem. Phys. Lett.*, 2006, **420**, 166–170.
- 64 H. Tabata, M. Fujii, S. Hayashi, T. Doi and T. Wakabayashi, *Carbon*, 2006, **44**, 3168–3176.
- 65 A. Lucotti, M. Tommasini, M. Del Zoppo, C. Castiglioni, G. Zerbi, F. Cataldo, C. S. Casari, A. Li Bassi, V. Russo, M. Bogana and C. E. Bottani, *Chem. Phys. Lett.*, 2006, **417**, 78–82.
- 66 A. Hu, Q. B. Lu and W. W. Duley, *J. Chem. Phys.*, 2007, **126**, 154705.

- 67 F. Cataldo and Y. Keheyan, *Fullerenes, Nanotubes, Carbon Nanostruct.*, 2002, **10**, 313–332.
- 68 A. Hu and W. W. Duley, *Chem. Phys. Lett.*, 2008, **450**, 375–378.
- 69 J. C. S. Costa, A. C. Sant'Ana, P. Corio and M. L. A. Temperini, *Talanta*, 2006, **70**, 1011–1016.
- 70 H. Shinohara, Y. Yamakita and K. Ohno, *J. Mol. Struct.*, 1998, **442**, 221–234.
- 71 K. Ohno, R. Takahashi, M. Yamada and Y. A. Isogai, *J. Mol. Des.*, 2002, **1**, 636–658, <http://www.biochempress.com>.
- 72 C. W. Bauschlicher Jr, E. Peeters and L. J. Allamandola, *Astrophys. J.*, 2009, **697**, 311–327.
- 73 I. Cherchneff, J. R. Barker and A. G. Tielens, *Astrophys. J.*, 1992, **401**, 269–287.
- 74 K. Habiba, V. I. Makarov, J. Avalos, M. J. F. Guinel, B. R. Weiner and G. Morell, *Carbon*, 2013, **64**, 341–350.